International Journal of Solids and Structures 50 (2013) 246–255

Contents lists available at SciVerse ScienceDirect

International Journal of Solids and Structures

journal homepage: www.elsevier.com/locate/ijsolstr

The micropolar elastic behaviour of model macroscopically heterogeneous materials

A.J. Beveridge, M.A. Wheel *, D.H. Nash

Department of Mechanical Engineering, University of Strathclyde, Glasgow G1 1XJ, UK

ARTICLE INFO

Article history:
Received 1 May 2012
Received in revised form 17 September 2012
Available online 3 October 2012

Keywords:
Heterogeneous material
Micropolar elasticity
Size effect

ABSTRACT

This paper describes the design, manufacture, testing and analysis of two model heterogeneous materials that exhibit non classical elastic behaviour when loaded. In particular both materials demonstrate a size effect in which stiffness increases as test sample size reduces; an effect that is unrecognized by classical elasticity but predicted by more generalized elasticity theories that are thought to describe the behaviour of heterogeneous materials more fully. The size effect has been observed by both experimental testing and finite element analysis that fully incorporates the details of the underlying heterogeneity designed into each material. The size effect has been quantified thus enabling both the modulus and also the characteristic length, an additional constitutive parameter present within micropolar and other generalized elasticity theories, to be determined for each material. These characteristic length values are extraordinarily similar to the length scales associated with the structure of the materials. An additional constitutive parameter present within plane micropolar elasticity theory that quantifies shear stress asymmetry has also been determined for one of the materials by using an iterative process that seeks to minimize the differences between numerical predictions and test results.

1. Introduction

Most materials are usually heterogeneous; they are composed of an underlying structure that can be observed at some scale. Nevertheless, while the constitutive behaviour may vary from point to point this variation can be ignored because the size scale of the heterogeneity is insignificant; the overall behaviour can then be regarded as an averaging of any pointwise variation. This homogenization is assumed in constitutive theories such as classical elasticity (Sadd, 2005) which also assumes locality in that the state of stress at any point in a loaded material only depends on the state of strain there. However, when the scale of the underlying structure is comparable to the overall scale then the assumption of homogeneity may be invalid. This can occur in traditional materials such as ceramics and cement, more recently developed materials like particulate and short fibre reinforced composites and modern cellular and honeycomb materials (Gibson and Ashby, 1999) which are now being used ever more extensively because of the weight saving they afford. It can also arise in naturally occurring materials like wood, bone and rock and when supposedly homogeneous materials are used to manufacture micro mechanical systems. The consequences of material heterogeneity are believed to include size effects in which stiffness increases as overall size is reduced, modified elastic wave propagation and alteration of localized stress concentrations. More general theories of elasticity that account for material heterogeneity and predict these effects have been developed. These theories can be categorized into two broad classes; those that incorporate higher derivatives of displacement or strain gradients into the constitutive relations (Maugin and Metrikine, 2010) and those that incorporate additional degrees of freedom. The latter class includes Cosserat or micropolar elasticity (Sadd, 2005; Maugin and Metrikine, 2010; Eringen, 1966, 1999; Nowacki, 1972) in which rotational degrees of freedom that are independent of the conventional displacements are also included. These theories are inherently nonlocal and one of their common features is the inclusion of a length scale; an additional constitutive parameter that quantifies the size of the variation in the underlying structure and which must be measured by experiment. Other parameters may also have to be identified depending on the theory.

Experimental methods for determining the constitutive properties of expectedly micropolar materials based upon measuring size effects have been reported (Gauthier and Jahsman, 1975; Gauthier, 1981; Yang and Lakes, 1982; Lakes, 1983, 1986, 1995; Anderson and Lakes, 1994). Generally, these methods involve loading samples of material of similar geometry but varying size and identifying any variation in stiffness with size. Constitutive properties are then determined by comparing experimental observations of the size effect with analytical predictions for the particular loading mode employed. Identifying all the relevant parameters would usually involve testing in more than one loading mode, typically beam bending and torsion of rods. However, early attempts to identify size effects in a model material fabricated by encapsulating

* Corresponding author. Tel.: +44 141 548 3307; fax: +44 141 552 5105.
E-mail address: marcus.wheel@strath.ac.uk (M.A. Wheel).

0020-7683/$ - see front matter © 2012 Elsevier Ltd. All rights reserved.
http://dx.doi.org/10.1016/j.ijsolstr.2012.09.023

aluminium shot particles within an epoxy polymer matrix proved inconclusive (Gauthier, 1981); torsion test results produced considerable scatter and hinted that an anti size effect in which stiffness decreased with reducing sample size might be present. The inconsistency of this result has, in part, been explained by more recent theoretical work (Bigoni and Drugan, 2007) which indicates that for a heterogeneous material to exhibit micropolar behaviour the inclusions must be more compliant than the surrounding matrix and relatively dilute. Testing of real materials to identify their micropolar properties has also been conducted and results obtained for both polymeric foams (Lakes, 1986) and bone (Yang and Lakes, 1982). An elaborate experimental technique incorporating electromagnetic loading was employed to negate any local effects that mechanical loads would impose on the extremely small samples. Of the polymeric materials dense polyurethane foam appeared to exhibit micropolar behaviour while a syntactic or filled foam containing more rigid inclusions did not; an outcome that again concurs with theory. The need for careful sample preparation has also been reported (Anderson and Lakes, 1994); surface damage induced during the manufacture of closed cell polymethacrylimide samples was suggested as the cause of the observed size softening rather than the size stiffening anticipated. A method that identifies micropolar materials while negating the need to test samples of varying sizes has also been published (Lakes et al., 1985). This method relies on observing the opening of a crack located on the edge of a prismatic sample when twisted since crack opening will be displayed by a micropolar material but not by a homogeneous material.

In addition to the experimental effort that has been spent on attempting to identify the constitutive behaviour of heterogeneous materials considerable theoretical endeavour has also been expended in predicting behaviour by microstructural mechanics approaches. This work is particularly pertinent to understanding emerging micro and nano technological devices and structures. In general these endeavours attempt to represent materials at the microstructural level as some form of lattice structure that can then be represented by an assembly of individual elements. By considering an appropriate part of the assembly constitutive properties can then be estimated. Approaches of this type have been comprehensively reviewed previously (Ostoja-Starzewski, 2002).

The present paper examines the behaviour of another model micropolar material formed by introducing a repeated pattern of voids into an otherwise homogeneous material. The scale of the heterogeneity that the voids introduce was deliberately chosen so that the required range of material specimen sizes could all be loaded using commonplace mechanical testing equipment. In addition, the regularity of the void pattern facilitated finite element (FE) simulation of the material by using the element mesh to represent the solid matrix encapsulating the voids. This kind of detailed FE simulation affords the opportunity to investigate the effect of void distribution and volume fraction upon material behaviour without recourse to exhaustive experimentation.

Before describing the manufacture, testing and FE simulation of the model material a brief overview of micropolar elasticity is included for completeness. Simplifications of the general three dimensional constitutive equations are presented for both the planar case and also for that of a slender beam in bending.

2. Micropolar elasticity: an overview

In linear, three dimensional, micropolar elasticity the force stresses, τ_{ij}, and couple stresses, m_{ij}, are related to the deformations by (Eringen, 1966):

$$\tau_{ij} = \lambda\varepsilon_{kk}\delta_{ij} + (2\mu^* + \kappa)\varepsilon_{ij} + \kappa e_{ijk}(\theta_k - \phi_k) \tag{1}$$

$$m_{ij} = \alpha\phi_{k,k}\delta_{ij} + \beta\phi_{i,j} + \gamma\phi_{j,i} \tag{2}$$

where the strain components, ε, are given in terms of the displacements, u, and microrotations, ϕ, by:

$$\varepsilon_{ij} = u_{j,i} + e_{jik}\phi_k \tag{3}$$

while θ are the conventional macrorotations, δ is the Kronecher delta symbol, e is the permutation tensor and the repeated indices denote summation over the range (i, j, k = 1, 2, 3). The six elastic constants, λ, μ^*, κ, α, β, and γ can be reinterpreted in terms of the engineering constants, E_M, G_M, υ_M, l_b, l_t, N and Ψ (Gauthier and Jahsman, 1975; Lakes, 1995) where the first three of these correspond to the Young's modulus, shear modulus and Poisson's ratio that govern uniform dilatational and distortional straining in a micropolar material as they do in classical elasticity. The subscript M is used here to distinguish them from their classical counterparts. The constants l_b and l_t are the characteristic lengths in bending and torsion respectively. In micropolar elasticity orthogonal shear stresses need not be complementary, any asymmetry being balanced by the couple stresses. The coupling number, N, then characterizes the asymmetry. The polar ratio, Ψ, plays a role akin to Poisson's ratio but relates orthogonal microrotations rather than dilatational strains.

In two dimensional Cartesian coordinates the strain displacement relations (3) can be expanded thus (Nakamura and Lakes, 1995):

$$\begin{pmatrix}\varepsilon_{xx}\\ \varepsilon_{yy}\\ \varepsilon_{yx}\\ \varepsilon_{xy}\end{pmatrix} = \begin{pmatrix}u_{x,x}\\ u_{y,y}\\ u_{x,y} + \phi_z\\ u_{y,x} - \phi_z\end{pmatrix} \tag{4}$$

and if the membrane in a state of plane stress Eqs. (1) and (2) can be expressed as:

$$\begin{pmatrix}\tau_{xx}\\ \tau_{yy}\\ \tau_{yx}\\ \tau_{xy}\end{pmatrix} = \begin{pmatrix}\frac{(2\lambda+2\mu^*+\kappa)(2\mu^*+\kappa)}{(\lambda+2\mu^*+\kappa)} & \frac{\lambda(2\mu^*+\kappa)}{(\lambda+2\mu^*+\kappa)} & 0 & 0\\ \frac{\lambda(2\mu^*+\kappa)}{(\lambda+2\mu^*+\kappa)} & \frac{(2\lambda+2\mu^*+\kappa)(2\mu^*+\kappa)}{(\lambda+2\mu^*+\kappa)} & 0 & 0\\ 0 & 0 & \mu^*+\kappa & \mu^*\\ 0 & 0 & \mu^* & \mu^*+\kappa\end{pmatrix}\begin{pmatrix}\varepsilon_x\\ \varepsilon_y\\ \varepsilon_{yx}\\ \varepsilon_{xy}\end{pmatrix} \tag{5}$$

and

$$\begin{pmatrix}m_{xz}\\ m_{yz}\end{pmatrix} = \begin{pmatrix}\gamma & 0\\ 0 & \gamma\end{pmatrix}\begin{pmatrix}\phi_{z,x}\\ \phi_{z,y}\end{pmatrix} \tag{6}$$

or in terms of the engineering constants as:

$$\begin{pmatrix}\tau_{xx}\\ \tau_{yy}\\ \tau_{yx}\\ \tau_{xy}\end{pmatrix} = \frac{E_M}{(1-\nu_M^2)}\begin{pmatrix}1 & \nu_M & 0 & 0\\ \nu_M & 1 & 0 & 0\\ 0 & 0 & \frac{(1-\nu_M)}{2(1-N^2)} & \frac{(1-\nu_M)(1-2N^2)}{2(1-N^2)}\\ 0 & 0 & \frac{(1-\nu_M)(1-2N^2)}{2(1-N^2)} & \frac{(1-\nu_M)}{2(1-N^2)}\end{pmatrix}\begin{pmatrix}\varepsilon_x\\ \varepsilon_y\\ \varepsilon_{yx}\\ \varepsilon_{xy}\end{pmatrix} \tag{7}$$

and

$$\begin{pmatrix}m_{xz}\\ m_{yz}\end{pmatrix} = \begin{pmatrix}\frac{2E_M l_b^2}{1+\nu_M} & 0\\ 0 & \frac{2E_M l_b^2}{1+\nu_M}\end{pmatrix}\begin{pmatrix}\phi_{z,x}\\ \phi_{z,y}\end{pmatrix} \tag{8}$$

since in this case the out of plane force and couple stress components, τ_{xz}, τ_{yz}, τ_{zx}, τ_{zy}, τ_{zz}, m_{xy}, m_{yx}, m_{zx} and m_{zy} are all zero as are ϕ_x and ϕ_y, the microrotations about the x and y axes respectively.

Fig. 1 shows the components of force stress and couple stress acting on a differential element in the membrane. Static equilibrium of the element is described by two translational equilibrium equations as in classical elasticity:

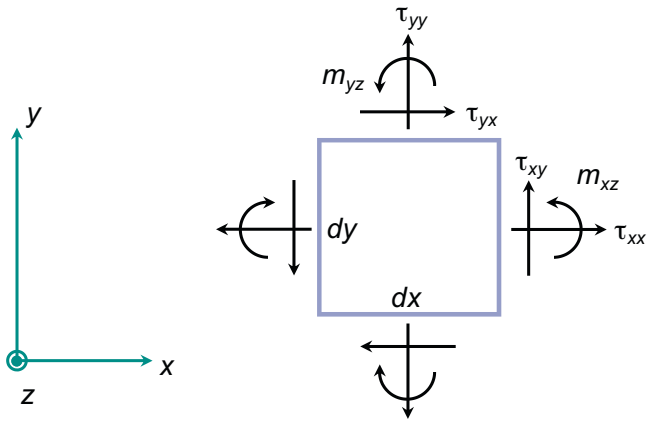

Fig. 1. Force stresses and couple stresses acting on plane material element.

$$\tau_{xx,x} + \tau_{yx,y} + p_x = 0 \tag{9}$$

$$\tau_{yy,y} + \tau_{xy,x} + p_y = 0 \tag{10}$$

and an additional rotational equilibrium equation:

$$m_{xz,x} + m_{yz,y} + \tau_{xy} - \tau_{yx} + q_z = 0 \tag{11}$$

that balances the couple stresses and antisymmetric shear stresses. Here p_x, p_y and q_z are the body forces and moment per unit volume respectively. The shear stresses can be partitioned into a symmetric component, τ_s, and an antisymmetric component, τ_a thus:

$$\tau_{xy} = \tau_s + \tau_a \tag{12}$$

and

$$\tau_{yx} = \tau_s - \tau_a \tag{13}$$

or

$$\tau_s = 1/2(\tau_{xy} + \tau_{yx}) \tag{14}$$

and

$$\tau_a = 1/2(\tau_{xy} - \tau_{yx}) \tag{15}$$

Fig. 2 shows the deformations that the shear stresses impose on the differential element; the symmetric component is associated with the conventional macrorotation, θ_z (=$u_{y,x} - u_{x,y}$), while the antisymmetric part is associated with the microrotation, ϕ_z. When $N = 0$ the shear stresses are complementary and the constitutive behaviour tends to the classical case which constitutes the lower bound of micropolar elasticity. The upper bound, when $N = 1$; is usually termed couple stress elasticity and in this case the microrotation, ϕ_z, equals the macrorotation, θ_z.

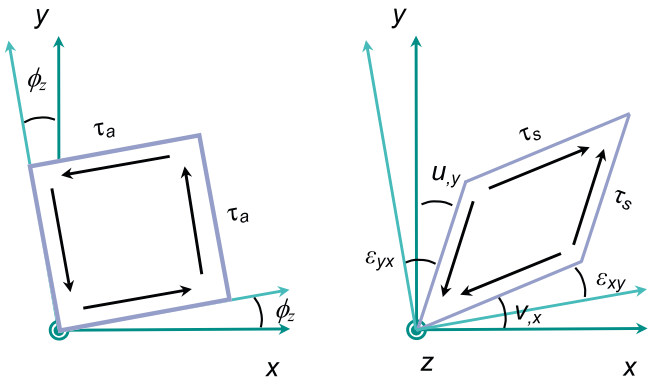

Fig. 2. Action of the shear stresses on the material element.

Assuming that a narrow, slender beam loaded in bending as in Fig. 3 is essentially two dimensional and that out of plane displacements, u_z, along with microrotations about in plane axes, ϕ_x and ϕ_y, can therefore be ignored, any externally applied moment, M, is then only resisted by the internal force stress, τ_{xx}, and the couple stress, m_{xz}, thus:

$$M = \int_A (y\tau_{xx} + m_{xz})dA \tag{16}$$

where A is the cross sectional area of the beam and y the distance from the neutral axis. This two dimensional analysis of a beam of rectangular cross section is thus a simplification of the full representation incorporating out of plane effects summarized previously (Lakes, 1995). One consequence of this simplification is that the micropolar and couple stress cases are indistinguishable. In addition, the beam structure is assumed to be composed of a material exhibiting isotropy at least within the two dimensional plane being considered, that is, it is transversely isotropic. The implications of these simplifying assumptions are discussed later.

The force stress is given by:

$$\tau_{xx} = \frac{E_{FM} y}{R} \tag{17}$$

in which the additional subscript F distinguishes a modulus obtained from a flexural test from that obtained in a uniaxial test. From Eq. (6) the couple stress is:

$$m_{xz} = \gamma \frac{d\phi_z}{dx} \tag{18}$$

where for a beam in pure bending being bent through a small angle, the radius of curvature, R, is:

$$\frac{1}{R} = \frac{d\theta}{dx} = \frac{d\phi_z}{dx} = -\frac{d^2 u_y}{dx^2} \tag{19}$$

By substituting (17) and (18) into (16) and using (19) to replace $1/R$ the moment curvature relationship:

$$\frac{d^2 u_y}{dx^2} = -\frac{M}{E_{FM} I + \gamma A} \tag{20}$$

is obtained for the beam where the second moment of area, I, and the cross sectional area, A, are defined as:

$$I = \int_A y^2 dA \tag{21}$$

and

$$A = \int_A dA \tag{22}$$

respectively. If Eq. (20) is solved for a beam of length L loaded by a centrally applied load W in three point bending then the central, maximum deflection, $\hat{u}_y$, is found to be:

$$\hat{u}_y = \frac{WL^3}{48(E_{FM} I + \gamma A)} \tag{23}$$

If the beam has a rectangular cross section of breadth, b, and depth, d, its stiffness, K, is then:

$$K = 4E_{FM} b \left(\frac{d}{L}\right)^3 \left[1 + \left(\frac{l_b}{d}\right)^2\right] \tag{24}$$

where the characteristic length in bending, l_b, is now related to the couple modulus, γ, by:

$$l_b = \sqrt{\frac{12\gamma}{E_{FM}}} \tag{25}$$

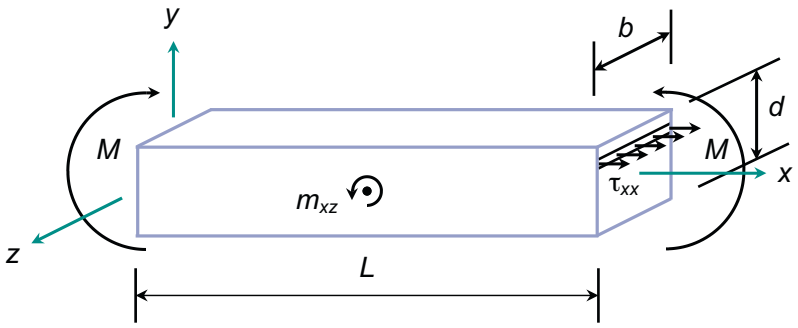

Fig. 3. Force stress, couple stress and bending moment acting on a micropolar beam.

Eq. (24) can be utilized in a size effect based approach to determining both the flexural modulus, E_{FM}, and characteristic length of a micropolar material. If slender beam samples of differing length but the same breadth and aspect ratio, L/d, are loaded in three point bending and their stiffnesses measured the variation in stiffness with the reciprocal of depth squared can then be determined. For a micropolar material this variation should be linear and its modulus can then be determined from the intercept with the stiffness axis while the characteristic length can be found from the gradient. For a classically elastic material the stiffness should be independent of size so the gradient will be zero implying that the characteristic length is also zero. To confirm whether this behaviour will be exhibited in practice a model micropolar material has been created. The model material offers two important advantages over a real material; its structure can be scaled such that it can be loaded using commonplace mechanical testing equipment and the regular nature of the heterogeneity lends itself to fully detailed modelling of the geometry of the structure constituting the material using FEA.

3. Model material

3.1. Manufacture

The model material samples were manufactured by machining an array of circular holes or voids into aluminium bar stock. Standard bars of depths 12.7, 25.4, 38.1 and 50.8 mm and a common breadth of 12.7 mm were used to manufacture beam samples of four different sizes. All bar stock was 6082 T6 aluminium alloy with a modulus of 70 GPa. To address the slender beam requirement the length of the samples was sufficient to ensure that they could each be tested at an aspect ratio of approximately 10:1. The holes were drilled through the breadth of the samples in a repeated hexagonal pattern. Two material densities were created by using a different hole separation, or pitch, along the sample length for each density. To negate surface effects the depthwise pitch was selected such that no holes intersected the upper or lower surfaces of any of the four samples of each material. The hexagonal pattern and associated pitches of the voids are illustrated in Fig. 4 while Table 1 lists these dimensions for both the high mass density (HMD) and low mass density (LMD) materials. Table 2 lists the dimensions of the four samples that were manufactured for each density of material while Fig. 5 depicts the four HMD samples. A material with a regular hexagonal pattern of voids is expected to be transversely isotropic. For the HMD material the void are arranged in an almost regular manner so the material should exhibit in plane isotropic behaviour. However, in the case of the LMD material the pitches specified in Table 1 result in a less regular void arrangement and therefore the material is expected to exhibit a greater degree of anisotropy.

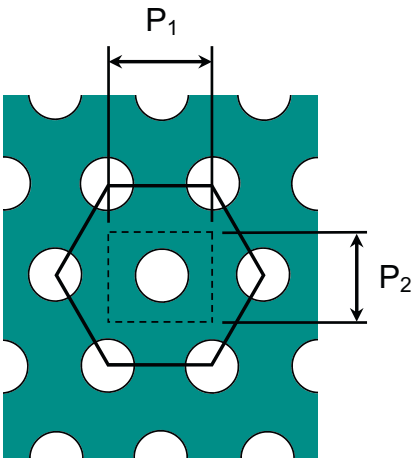

Fig. 4. Horizontal pitch, P_1, and vertical pitch, P_2, of voids in model material.

Table 1
Void radius, r, horizontal pitch, P_1, and vertical pitch, P_2, for HMD and LMD model materials.

Beam	r (mm)	P_1 (mm)	P_2 (mm)
HMD	3.5	16	12.7
LMD	3.5	9	12.7

Table 2
Beam dimensions of HMD and LMD test pieces.

Beam	Breadth (mm)	Depth (mm)	Length (mm)
B1	12.7	12.7	150
B2	12.7	25.4	280
B3	12.7	38.1	400
B4	12.7	50.8	530

3.2. Slender beam testing

All four samples of both materials were loaded in three point bending in a Zwick 2061 hydraulic tensile testing machine with a 50 kN load cell. The supports on which the samples rested were attached to a base plate that was connected to the lower, moving crosshead of the machine. The separation of the supports was adjusted for each size of sample to maintain a constant aspect ratio for all sample sizes. For all samples both of the supports were positioned midway between horizontally adjacent voids to minimise the effect of loading on sample deformation local to each support. Consequently the aspect ratio used to test the HMD samples was

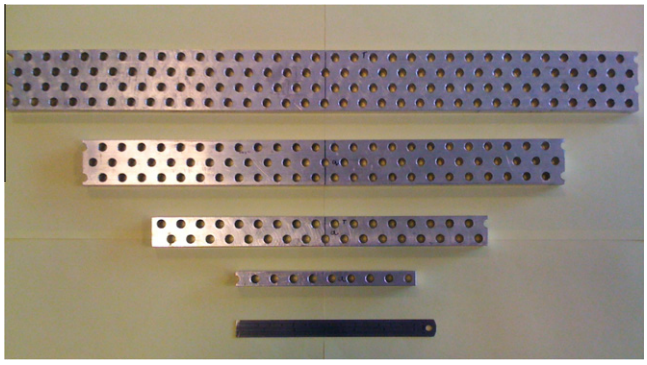

Fig. 5. High mass density beam test pieces of model material.

slightly greater than 10 (10.08) while for the LMD samples it was a little less than 10 (9.92). The central load was applied to each sample midway between neighbouring holes by the upper, stationary machine crosshead in which the load cell was located. In order to ensure that the displacement of the sample was accurately measured, so that the correct stiffness could be ascertained, the central deflection was measured relative to the supports. This was achieved by placing a bar across the supports in parallel to the sample so that during loading a displacement transducer was used to monitor the difference between the central deflection of the sample and the bar which remained unloaded throughout. In this way the effect of any deformation of the end supports and plate to which they were attached could be eliminated.

3.3. FE modelling

Alongside the experimental testing detailed FE analysis of all four samples, of both the HMD and LMD materials, was performed using the commercially available FE package ANSYS. FE meshes of each sample were generated by firstly meshing one quarter of a rectangular region or cell surrounding a given void as shown in Fig. 6. This mesh was then reflected about axes aligned with the horizontal and vertical ligaments to produce a mesh bounded by the rectangle and enclosing the void. This mesh was then replicated at repeated horizontal and vertical pitch increments as required to mesh a complete sample. Coincident nodes were merged after each replication to ensure correct connectivity of the complete mesh. All meshes were generated using 8 noded quadrilateral elements.

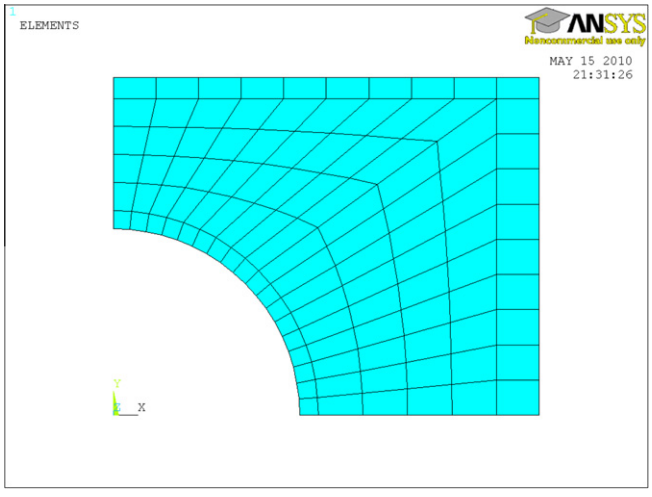

Fig. 6. Finite element mesh around individual void.

Young's modulus and Poisson's ratio values of 70.0 GPa and 0.3, respectively were assigned to each element material type and linear elastic behaviour was assumed. Convergence of the predicted central displacement with mesh refinement was investigated by progressively increasing the number of element divisions along the lines defining the perimeter of the quarter cell. For the largest sample size of the HMD and LMD materials meshes containing 7136 and 10,512 nodes respectively provided sufficiently accurate displacement predictions. The larger mesh size required for the LMD material results from having the same number of nodes along the ligaments of the quarter cell for both materials. Constraints were applied by fixing both displacement components at the node corresponding to one of the support points but only the vertical displacement at the node coincident with the other support. A point nodal load was applied to the top edge of the beam at mid span. The stiffness value of each beam was calculated by averaging the predicted vertical displacements of the nodes located at mid span and dividing this by the applied load. The variation in predicted vertical displacement was minimal except locally at the point of load application where it was found to vary by up to 5% at most. Averaging in this manner was therefore thought to provide the most representative estimate of sample stiffness.

4. Results

The measured and predicted variations in beam stiffness with sample size, quantified by the measure $1/d^2$, are shown in Figs. 7 and 8 for the HMD and LMD respectively. These figures also show the variation in stiffness expected from samples of classically elastic materials with the same modulii as the model materials. For the HMD material the experimentally measured and predicted stiffnesses are generally in close agreement but there is discrepancy of approximately 2.5% between the values obtained for the smallest sample. For the LMD material a similar correlation is observed although in this case there is a difference of nearly 6.5% between the measured and predicted stiffnesses for the second smallest sample. Nevertheless, despite these minor disparities the test results presented in these two figures along with the corroborating predictions obtained by FE analysis clearly demonstrate that both materials exhibit a size effect of the kind forecast by Eq. (24) for a micropolar medium. Interestingly, even the smallest samples of each material appear to follow the forecast effect in spite of the uncertainty concerning the applicability of transverse isotropic continuum behaviour in samples of this size.

Flexural modulus and characteristic length values were determined for both materials using Eq. (24) along with a linear fit of

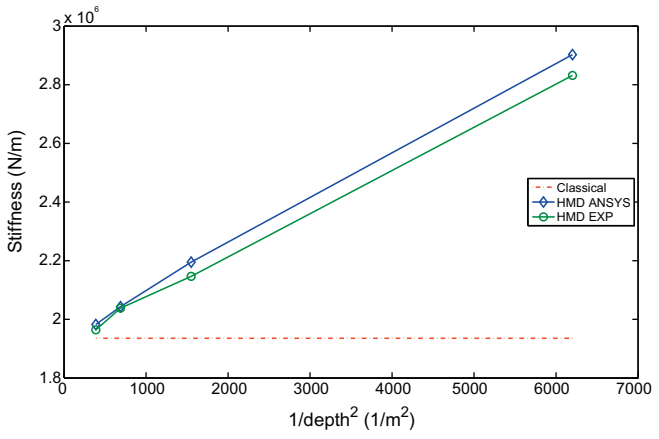

Fig. 7. Measured and predicted variations in beam stiffness with sample size, $1/d^2$, for HMD material at $L/d = 10.08$.

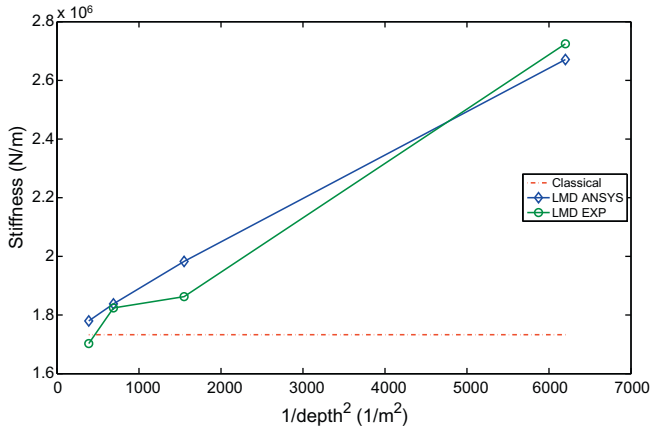

Fig. 8. Measured and predicted variations in beam stiffness with sample size, $1/d^2$, for LMD material at $L/d = 9.92$.

the measured and predicted stiffness data presented in Figs. 7 and 8. The values obtained for the HMD and LMD materials are listed in Tables 3 and 4 respectively. The consistency between the values obtained from the measured and predicted stiffness data is evident from both tables. Additionally, a comparison between tables reveals that for the LMD material the modulus is reduced while the characteristic length is increased. The first of these observations is understandable given that in the LMD case the void volume fraction is greater and hence there is less material matrix to support any applied load. The second implies a greater degree of heterogeneity in the LMD material. The other notable observation from the tables is the magnitude of the characteristic length values. According to micropolar elasticity theory this length characterises the range of the couple stresses and, as argued in the literature, should somehow reflect the physical size scale of the underlying structure in a heterogeneous material. The characteristic length values reported in the tables do exactly that; they represent some aggregated measure of the internal dimensions within the material, namely the hole diameter and pitch, rather than corresponding to one or other of these precisely.

4.1. Deep beam testing

Experimental testing and complementary FE analysis of slender HMD and LMD material beam samples loaded in three point bending has identified that both materials exhibit increasing flexural stiffness as sample size reduces. Additionally, the variation in stiffness with sample size exhibited by both materials is consistent with that expected of a material with micropolar or couple stress constitutive behaviour. Characteristic length values have been determined for both materials and these are similar to the physical length scales defining the underlying structure of each model material. However, the analysis of the slender beam tests used to generate these values does not differentiate between micropolar and couple stress behaviour. To identify this difference requires an enhancement in the shear deformation induced in the samples as they are loaded. This can be achieved by testing the same samples at a lower aspect ratio, that is, by reducing the span through moving the supports closer together. Fig. 9 illustrates the anticipated effect of testing samples at an aspect ratio of approximately 50% of that used previously. These predicted variations in sample stiffness with size were determined using a novel control volume based finite element procedure CV-MPLST that incorporates micropolar constitutive behaviour. The procedure is an enhancement of an earlier approach (Wheel, 2008) but incorporates the higher order displacement variations associated with linear strain triangular elements rather than constant strain triangles. Since the procedure incorporates micropolar constitutive behaviour the detailed representation of the void array within the samples was unnecessary and each sample could be represented by a rectangular region paved by a mesh of 80 identical right angled triangular elements with 10 element divisions in the spanwise direction and 4 through thickness. The flexural modulus and characteristic length values obtained from the slender beam tests were employed by the procedure to obtain the variations in stiffness with size for different values of the coupling number, N. Fig. 9 clearly shows that on approaching couple stress behaviour, represented approximately by $N = 0.9$, the stiffness variation remains linear and increases with reducing sample size, while for $N = 0$ the stiffness is independent of size as expected of a classically elastic material. However, for intermediate values of N the variation in stiffness lies somewhere between these bounds. Thus identifying the stiffness variation for lower aspect ratio samples experiencing greater shear deformation than the slender samples should provide a means of quantifying the coupling number of the model materials under investigation.

Three point bending tests were therefore performed on the same sets of HMD and LMD material samples, at aspect ratios of approximately 75% and 50% of the earlier value, using the same experimental procedure as employed previously. The particular aspect ratio values differed slightly for the two materials because of the desire to support each sample midway between adjacent horizontally spaced voids and minimize the effect of any localized deformation at the support points. In addition, an FE analysis of each test was

Table 3
Constitutive properties of HMD material obtained from linear fit to data presented in Fig. 7 (flexural modulus, E_{FM}, couple modulus, γ, and characteristic length of bending, l_b).

	E_{FM} (N/m^2)	γ (N)	l_b (mm)
EXP	3.871e10	2.469e5	8.75
ANSYS	3.900e10	2.629e5	8.99

Table 4
Constitutive properties of LMD material obtained from linear fit to data presented in Fig. 8 (flexural modulus, E_{FM}, couple modulus, γ, and characteristic length of bending, l_b).

	E_{FM} (N/m^2)	γ (N)	l_b (mm)
EXP	3.148e10	2.745e5	10.23
ANSYS	3.310e10	2.416e5	9.36

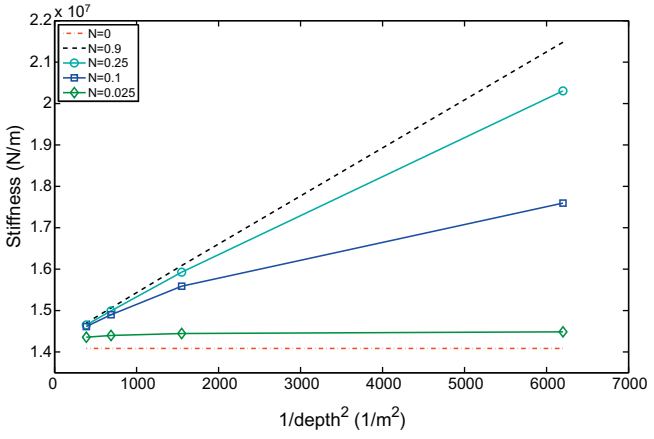

Fig. 9. Predicted variations in HMD beam stiffness with sample size, $1/d^2$, for various coupling numbers, N, at $L/d = 5.04$.

again undertaken to provide a prediction of the sample stiffness that could be compared to the experimentally determined value.

Figs. 10 and 11 show the measured and predicted variations in stiffness for the HMD material at sample aspect ratios of 7.56:1 and 5.04:1, respectively. Similarly, the stiffness variations for the LMD material determined experimentally and numerically at aspect ratios of 8.50:1 and 5.67:1 are shown in Figs. 12 and 13. Superimposed on all four figures are the variations in stiffness predicted by CV-MPLST using the constitutive properties obtained from slender beam testing and assuming classically elastic ($N = 0$) and approximate couple stress ($N = 0.9$) constitutive behaviour.

The first observation that is qualitatively evident from all four figures is that the variations in stiffness depart from those anticipated by couple stress elasticity theory and lie somewhere between this case and the classically elastic case for the smaller samples at least. Qualitative comparisons of Fig. 10 with Figs. 11 and 12 with 13 indicate that the departure from couple stress theory is accentuated by a reduction in sample aspect ratio implying that as the degree of shear deformation is increased the behaviour of both model materials is genuinely micropolar.

More quantitatively, Fig. 10 shows that the agreement between the measured and predicted stiffnesses for the HMD material at $L/d = 7.56$ is excellent. However, for the lower aspect ratio samples of both materials there is an offset between the FE and measured results with the latter being consistently lower than the former as seen in both Figs. 11 and 13. In these cases, slight indenting of the samples was observed after testing at the points resting on the supports indicating that a degree of localized plastic deformation had occurred there. The additional compliance actually accruing as a result of this deformation is not accounted for by the linear elastic FE analysis and hence the predicted stiffnesses are slightly greater than their measured counterparts.

The other quantitative observation of note is that for the lower aspect ratio LMD samples both the numerically predicted and measured stiffnesses of the larger samples are lower than anticipated by both couple stress and classical elasticity. FE analysis of uniaxially loaded flat plates containing the same void distributions as the HMD and LMD materials revealed that while the predicted angular variation in modulii was minimal for the former it reduced by over 25% from the axial to the through depth direction for the latter. Therefore, as anticipated when manufacturing the specimens the HMD material is approximately isotropic while the LMD possesses significant anisotropy. The stiffness variations anticipated by couple stress and classical elasticity shown in Fig. 9 assume isotropy. For a slender beam loaded in bending and satisfying the assumptions of Eq. (16) the influence of material anisotropy is minimal because the resulting deformation is largely governed by spanwise constitutive properties. However, this influence becomes more marked as slenderness is reduced because the state of stress becomes more complex than that assumed in Eq. (16). Consequently, both the numerically predicted and measured stiffnesses of the LMD samples are lower than theoretically anticipated.

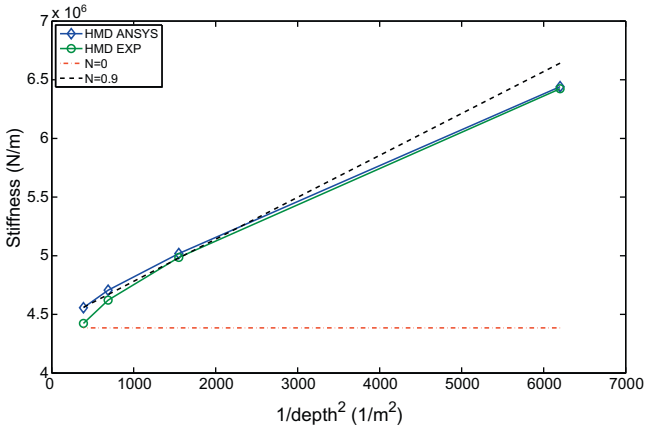

Fig. 10. Measured and predicted variations in beam stiffness with sample size, $1/d^2$, for HMD material at $L/d = 7.56$.

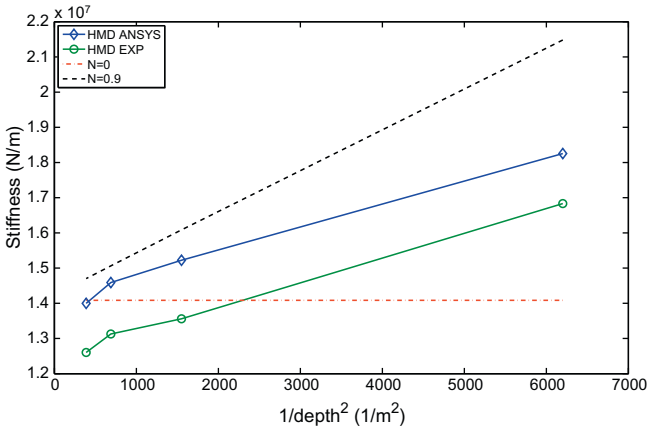

Fig. 11. Measured and predicted variations in beam stiffness with sample size, $1/d^2$, for HMD material at $L/d = 5.04$.

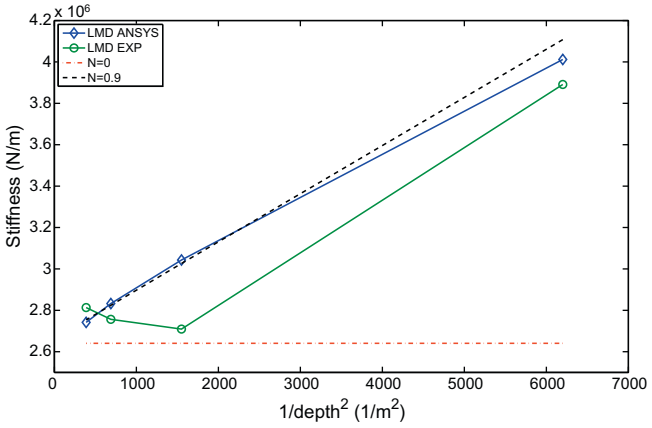

Fig. 12. Measured and predicted variations in beam stiffness with sample size, $1/d^2$, for LMD material at $L/d = 8.50$.

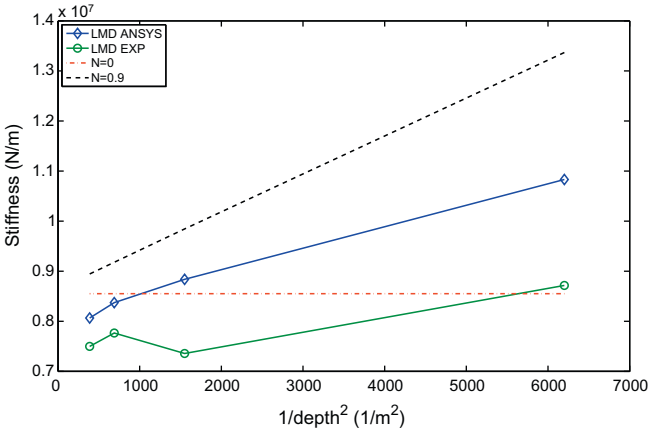

Fig. 13. Measured and predicted variations in beam stiffness with sample size, $1/d^2$, for LMD material at $L/d = 5.67$.

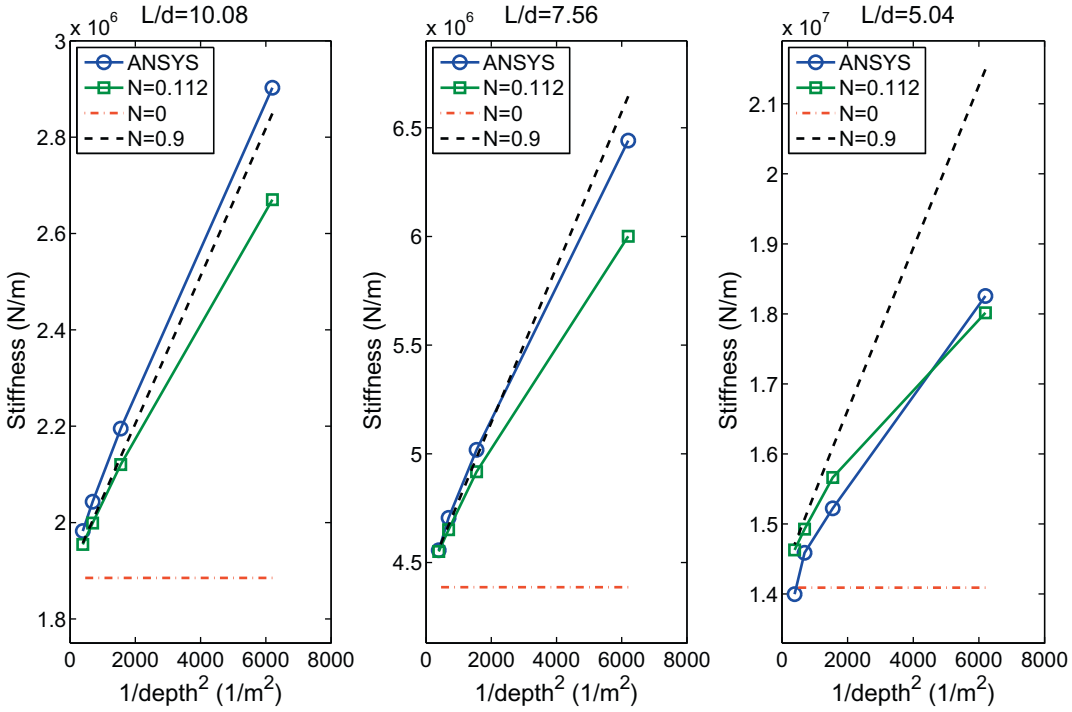

Fig. 14. Comparisons of numerically predicted stiffness values with FE results at three different sample aspect rations after identifying $N = 0.112$ using data for $L/d = 5.04$.

5. Identification of the coupling number, *N*, for HMD material

The results obtained from experimental testing and detailed FE analysis of deep beams of the two model materials has indicated that in both cases their constitutive behaviour is genuinely micropolar since the results lie within the bounds set by classical and couple stress elasticity theory. It should therefore be possible to use these results to quantify another parameter within the two dimensional constitutive equations (7), specifically the coupling number, *N*. However, there is apparently no analytical solution for the deflection of a deep rectangular cross sectioned micropolar beam undergoing simultaneous flexural and shearing deformation when loaded in three point bending. The approach that has therefore been adopted exploits the CV-MPLST procedure within an overall iterative process for solving the inverse system identification problem of quantifying the coupling number. Approaches of this type have been widely used in non destructive testing applications such as defect detection in load bearing structures (Bui, 1994) and also in constitutive property identification from materials tests (Husain, 2004; Partheepan et al., 2006).

The iterative process has been applied to determine the coupling number of the HMD material because it is more isotropic than its LMD counterpart and the CV-MPLST procedure assumes material isotropy. The process is fully automated and commences by applying a linear regression to the stiffness data obtained for the slender HMD material beams with $L/d = 10.08$. This yields the same data as given in Table 3. The process then enters an iterative cycle in which the constitutive property data yielded by the linear regression is used in conjunction with the CV-MPLST procedure and an initial value of the coupling number, *N*, to predict the stiffnesses of the four HMD material beams of shortest span with $L/d = 5.04$. For this CV-MPLST used a mesh of 10×4 triangular element to represent the beam geometry and assumed that Poisson's ratio, $\tilde{o}_m$, was equal to that of the aluminium matrix material, 0.3. A sensitivity analysis in which the value of $\tilde{o}_m$ was varied by ±15% demonstrated that the influence of this assumption was at most ±0.6% on predicted stiffnesses. Once CV-MPLST has predicted the stiffnesses of the samples these are then compared to the experimentally measured values or those obtained from the detailed FE analysis and an estimate of how well the predicted values match either of these is obtained by determining the coefficient of multiple determination, R^2. This is defined (Draper and Smith, 1966) as

$$R^2 = 1 - \frac{SS_{\text{err}}}{SS_{\text{tot}}} \tag{26}$$

where the sum of the squared residual errors, SS_{err}, is

$$SS_{err} = \sum (K_A - K_M)^2 \tag{27}$$

and the sum of the squared total errors, SS_{tot}, is

$$SS_{\text{tot}} = \sum (K_A - \bar{K}_A)^2 \tag{28}$$

K_A being the actual measured or FE predicted stiffnesses, K_M the estimated stiffnesses provided by the CV-MPLST procedure using the current value of *N* and $\bar{K}_A$ the mean of the actual stiffnesses. The actual and estimated stiffness data are the same when $R^2 = 1$. If, however, $R^2 < 1$ then the value of *N* is updated according to

$$N_{i+1} = \left[\frac{1}{n}\sum_{j=1}^{n}\frac{K_A}{K_M}\right] N_i \tag{29}$$

where *i* denotes the current iteration and *n* the number of data points. After updating the next iteration cycle commences. The cycle continues until either R^2 reaches a target value set to 0.99 at which point the process has assumed to have converged, or the R^2 value begins to diverge away from 1 whereby the point of divergence then indicating a best fit between the actual and estimated stiffness data. For the deep HMD beams with $L/d = 5.04$ the iterative process terminated when $R^2 = 0.93$ and $N = 0.112$. The right graph in Fig. 14 demonstrates that there is good agreement between the stiffness values predicted by the CV-MPLST procedure with this value of *N* and the actual stiffnesses of the four samples obtained from detailed FE analysis. However, when the procedure is used in conjunction with this value of *N* to predict the stiffness

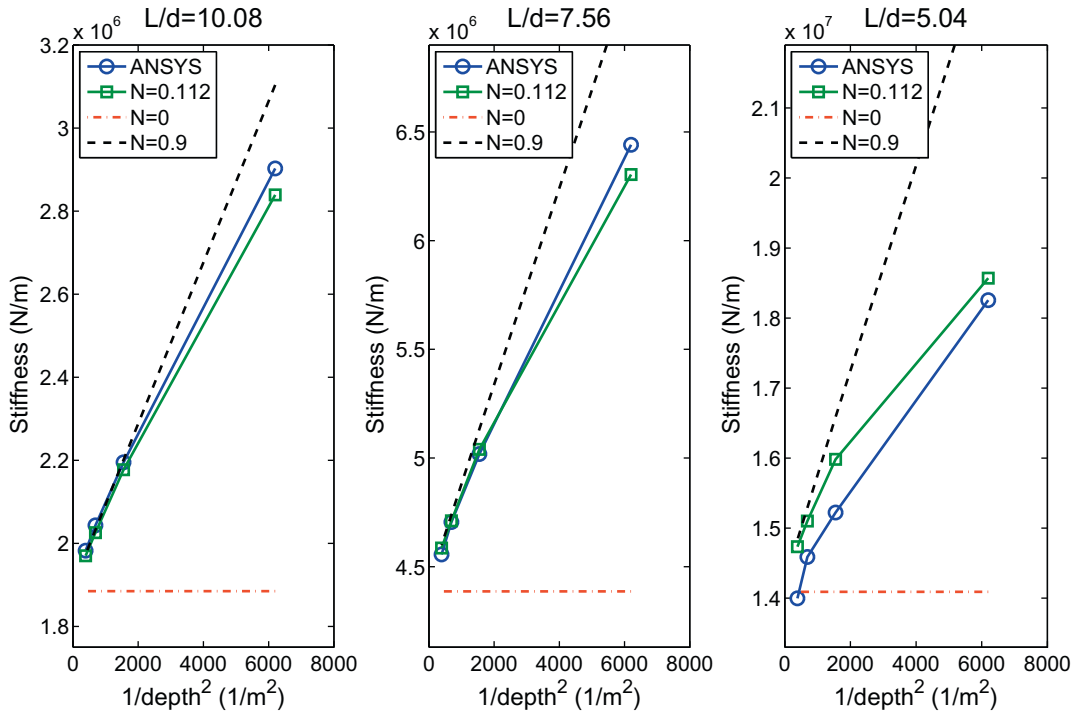

Fig. 15. Comparisons of numerically predicted stiffness values with FE results at three different sample aspect rations after identifying $\tilde{a} = 3.339 \times 10^5$ N using data for $L/d = 10.08$.

values of the more slender samples with $L/d = 7.56$ and $L/d = 10.08$ agreement is less satisfactory as illustrated in left and central graphs in Fig. 14.

To facilitate improved correlation between the predicted and actual data at the more slender aspect ratios the iterative process therefore incorporates a second stage that seeks to obtain an improved estimate of the couple modulus, $\tilde{a}$. This stage effectively acknowledges that the value of $\tilde{a}$ obtained initially from the linear regression is only approximate and relies on the assumption that the samples with $L/d = 10.08$ are sufficiently slender enough that their behaviour is accurately described by Eq. (24). The second stage emulates the first with the exception that Eq. (29) is used to update $\tilde{a}$ rather than N. When applied to the slender beam stiffness data iteration terminated with $R^2 = 0.99$ and $\tilde{a} = 3.339 \times 10^5$N. Fig. 15 compares the actual stiffnesses with the estimates obtained using this value of $\tilde{a}$ for the slender beams and also shows the effect this improved value has on predicted stiffness at the other two aspect ratios. These figure also incorporate a correction to the approximate, $N = 0.9$, upper bound resulting from the update in $\tilde{a}$. The figures show that at $L/d = 10.08$ and $L/d = 7.56$ agreement between actual and estimated stiffnesses is excellent while for the least slender beams agreement has diverged only slightly. For the $L/d = 10.08$ case it is interesting to note that reducing N significantly from 0.9 to 0.112 results in a reduction in stiffness of less than 10% for the smallest sample. The corresponding reduction in stiffness for the least slender samples is much more marked at over 20%. Thus it appears that for the slender samples the influence of N on the size effect is less significant and the distinction between the micropolar and couple stress cases is less pronounced. This observation thus appears to provide some support for the analysis used to derive equation (24) and the associated assumptions because no distinction between the two cases is anticipated by the analysis. Additional improvements in the constitutive property values identified could potentially be obtained by elaborating the iterative process further but this was deemed unnecessary. Thus the final constitutive data obtained for the HMD material are $E_{FM} = 39$ GPa, $N = 0.112$ and $\tilde{a} = 0.334$ MN giving $l_b = 10.14$ mm.

6. Conclusions

The model materials described in the present work were deliberately created to investigate the load bearing behaviour of plane heterogeneous continua by experiment and detailed finite element analysis. Experimental testing of beam samples loaded in bending has demonstrated that scaling down the sample size results in an increase in stiffness. This behaviour was confirmed by analysis. In general the experimentally and numerically determined sample stiffnesses were in agreement although the differences between them highlight the need for meticulous experimental data acquisition so that the stiffness variation and the constitutive data derived subsequently are accurately quantified. As already acknowledged (Lakes, 1986, 1995) the implications of this requirement will be even more exacting in the case of real materials where overall size scales and applied loading may be much smaller and corroborative numerical data unavailable.

Flexural modulus and characteristic length data have been derived for the materials from the observed size effect. The characteristic length values obtained are particularly noteworthy in that they are remarkably similar in magnitude to the intrinsic length scales designed into the materials. Forthcoming work will examine how the size and distribution of voids influences this constitutive property as well as the coupling number which was quantified for one of the materials investigated. The agreement between test and numerical results implies that finite element analysis rather than experimentation could justifiably form the basis of both this investigation and future work to identify the constitutive properties of genuinely three dimensional heterogeneous materials.

References

Anderson, W.B., Lakes, R.S., 1994. Size effects due to Cosserat elasticity and surface damage in closed-cell polymethacrylimide foam. Journal of Materials Science 29 (24), 6413–6419.

Bigoni, D., Drugan, W.J., 2007. Analytical derivation of Cosserat moduli via homogenization of heterogeneous elastic materials. Journal of Applied Mechanics 74 (4), 741–753.

Bui, H.D., 1994. Inverse Problems in the Mechanics of Materials: An Introduction. CRC Press.
Draper, N.R., Smith, H., 1966. Applied Regression Analysis. Wiley.
Eringen, A.C., 1966. Linear theory of micropolar elasticity. Journal of Mathematics and Mechanics 15 (6), 909–923.
Eringen, A.C., 1999. Microcontinuum Field Theories I: Foundations and Solids. Springer-Verlag, New York.
Gauthier, R.D., 1981. Experimental Investigations of Micropolar Media. World Scientific, Singapore.
Gauthier, R.D., Jahsman, W.E., 1975. A quest for micropolar elastic constants. Journal of Applied Mechanics 42, 369–374.
Gibson, L.J., Ashby, M.F., 1999. Cellular Solids. Cambridge University Press.
Husain, A., 2004. An inverse finite element procedure for the determination of constitutive tensile behavior of materials using miniature specimen. Computational Materials Science 31 (1–2), 84–92.
Lakes, R.S., 1983. Size effects and micromechanics of a porous solid. Journal of Materials Science 18 (9), 2572–2580.
Lakes, R.S., 1986. Experimental microelasticity of two porous solids. International Journal of Solids and Structures 22 (1), 55–63.
Lakes, R.S., 1995. Experimental methods for study of Cosserat elastic solids and other generalized elastic continua. In: Mühlhaus, H. (Ed.), Continuum Models for Materials with Micro-structure. Wiley, New York.
Lakes, R.S., Gorman, D., Bonfield, W., 1985. Holographic screening method for microelastic solids. Journal of Materials Science 20 (8), 2882–2888.
Maugin, G.A., Metrikine, A.V. (Eds.), 2010. Mechanics of Generalized Continua: One Hundred Years after the Cosserats. Springer.
Nakamura, S., Lakes, R.S., 1995. Finite element analysis of Saint-Venant end effects in micropolar elastic solids. Engineering Computations 12, 571–587.
Nowacki, W., 1972. Theory of Micropolar Elasticity. Springer-Verlag.
Ostoja-Starzewski, M., 2002. Lattice models in micromechanics. Journal of Applied Mechanics 55, 35–60.
Partheepan, G., Sehgal, D.K., Pandey, R.K., 2006. An inverse finite element algorithm to identify constitutive properties using dumb-bell miniature specimen. Modelling and Simulation in Materials Science and Engineering 14 (8), 1433–1445.
Sadd, M.H., 2005. Elasticity: Theory, Applications, and Numerics. Elsevier, Butterworth Heinemann.
Wheel, M.A., 2008. A control volume-based finite element method for plane micropolar elasticity. International Journal for Numerical Methods in Engineering 75 (8), 992–1006.
Yang, J.F.C., Lakes, R.S., 1982. Experimental study of micropolar and couple stress elasticity in bone in bending. Journal of Biomechanics 15, 91–98.